Development of a New Inanimate Class for the WSR-88D Hydrometeor Classification Algorithm

JAMES M. KURDZO, MARK S. VEILLETTE, BETTY J. BENNETT, DAVID J. SMALLEY, EARLE R. WILLIAMS, AND MICHAEL F. DONOVAN

MIT Lincoln Laboratory, Lexington, Massachusetts

ABSTRACT

The current implementation of the Hydrometeor Classification Algorithm (HCA) on the WSR-88D network contains two non-hydrometeor-based classes: ground clutter/anomalous propagation and biologicals. A number of commonly observed non-hydrometeor-based phenomena do not fall into either of these two HCA categories, but often are misclassified as ground clutter, biologicals, unknown, or worse yet, weather hydrometeors. Some of these phenomena include chaff, sea clutter, combustion debris and smoke, and radio frequency interference. In order to address this discrepancy, a new class (nominally named "inanimate") is being developed that encompasses many of these targets. Using this class, a distinction between non-biological and biological non-hydrometeor targets can be made and potentially separated into sub-classes for more direct identification. A discussion regarding the fuzzy logic membership functions, optimization of membership weights, and class restrictions is presented, with a focus on observations of highly stochastic differential phase estimates in all of the aforementioned targets. Recent attempts to separate the results into sub-classes using a support vector machine are presented, and examples of each target type are detailed. Details concerning eventual implementation into the WSR-88D radar product generator are addressed.

1. Introduction

The operational Hydrometeor Classification Algorithm (HCA) on the WSR-88D network serves as a tool for radar users to discriminate between different types of hydrometeors (Park et al. 2009). Radar users can differentiate among frozen and liquid hydrometeors, ground clutter, and biological targets. The HCA is useful for determining where mixed precipitation may be occurring (a melting layer or rain/snow line), if large/giant hail is occurring in a severe thunderstorm, and if targets above the melting layer consist of mainly dry/wet snow or ice crystals. The HCA was not designed to isolate mixed-phase conditions and only reports a single class per range bin.

The HCA was developed through years of experimentation (Ryzhkov et al. 2005) and theoretical analysis (Bringi and Chandrasekar 2005). It makes use of the polarimetric estimates available from the WSR-88D (Crum and Alberty 1993; Doviak et al. 2000), including differential reflectivity (Z_{DR}), cross-correlation coefficient (ρ_{HV}), and differential phase (Φ_{DP}). Through the use of a fuzzy logic algorithm, trapezoidal membership functions for different variables are combined with weights and quality vectors in order to determine the most likely target type. These membership functions and weights were derived using a myriad of techniques, with significant input coming from the Joint Polarization Experiment (JPOLE; Ryzhkov et al. 2005).

Currently, there are three non-hydrometeor classifications possible in the operational HCA: ground clutter/anomalous propagation, biologicals, and unknown (for no decision from the HCA). The unknown category is selected when the aggregation of membership functions does not reach a critical threshold for defining a single target type. An additional non-hydrometeor class, tornadic debris, is also currently being added to the HCA and will be available in the next year (Snyder and Ryzhkov 2015). However, there are numerous target types that don't fall into the ground clutter, biological, or tornadic debris classes that are commonly placed into these categories due to the lack of any other option. Some of these targets include military chaff, sea clutter, and combustion debris/smoke, as well as the occurrence of radio frequency interference (RFI).

The purpose of this paper is to detail the development of a new, singular "inanimate" class for the operational WSR-88D HCA that incorporates these four target types. These targets don't readily fall into ground clutter or biologicals, so it is sensible to include an additional class that separates them from these types of targets. Doing so would mitigate some of the false alarms of

Corresponding author address: James M. Kurdzo, Air Traffic Control Systems, MIT Lincoln Laboratory, 244 Wood Street, Lexington, MA 02421. E-mail: James.Kurdzo@ll.mit.edu

DISTRIBUTION STATEMENT A. Approved for public release: distribution unlimited. This material is based upon work supported by the Federal Aviation Administration under Air Force Contract No. FA8721-05-C-0002 and/or FA8702-15-D-0001. Any opinions, findings, conclusions or recommendations expressed in this material are those of the author(s) and do not necessarily reflect the views of the Federal Aviation Administration.

existing classifications brought on by misclassification of these four other non-hydrometeor phenomena.

2. Target Types and Characteristics

Military chaff has been utilized as a radar countermeasure around the world since World War II (De Martino 2012). Due to its metallic coating and lengths cut specifically to resonate at a given incident frequency of electromagnetic energy (Hessemer 1961; Palermo and Bauer 1965), chaff can generate substantial radar cross sections that disperse into large "clouds" of distributed targets (Pinson 1975; Harrison and Heinz 1963; Zrnić and Ryzhkov 2004; Fig. 1). These targets simulate broad returns to an enemy radar system, leading to the potential for masking aircraft, warships, and missiles from enemy detection (Pode 1960).

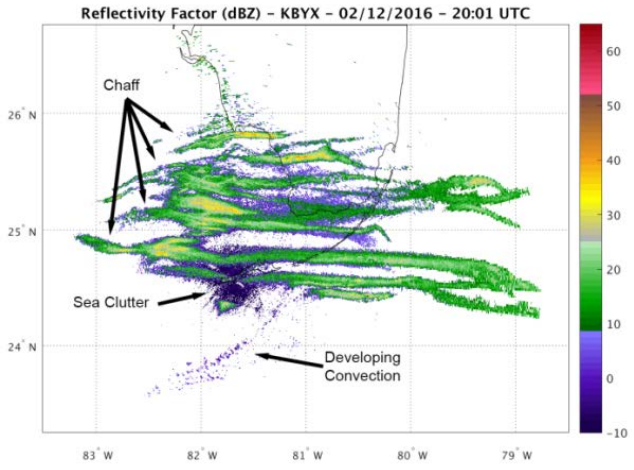

FIG 1: Bands of chaff (horizontal trails) in the reflectivity factor estimate on 12 February 2016 at the KBYX WSR-88D.

The utility and effectiveness of chaff has led to widespread use not only in the battlefield, but, logically, also as a training tool in the United States and abroad. Due to its prevalence in training exercises, evidence of chaff can often be found in radar returns across the national airspace in day-to-day aviation operations.

Sea clutter is similar to ground clutter in that it is evident during super-refraction conditions when the beam is bent towards the surface due to high refractivity gradients (Chan 1990). Unlike ground clutter, which can often be filtered using a notch filter at zero Doppler velocity (or other techniques; e.g., Torres and Zrnić 1999; Torres and Warde 2014), sea clutter has a non-zero Doppler component, resulting in considerable difficulty for filtering. For this reason, sea clutter is a tremendous contamination source for many types of radar systems.

Combustion debris and smoke result from surface-based fires, and can rise to exceptional levels above the ground (Melnikov et al. 2008; Jones and Christopher 2010). Ash consists of relatively large, reflective particles that resonate at the WSR-88D wavelength. Grass/brush fires, urban fires, and large wildfires are all sources of combustion debris that can reach the height of the radar beam if the boundary layer characteristics and range to the radar are ideal. As with chaff and sea clutter, smoke is generally considered a nuisance to forecasters, air traffic controllers, and automated algorithms, and can appear in a similar fashion to weather, leading to the desire to accurately identify its presence.

RFI is caused by interference from other transmitting sources in a radar's transmit/receive band, and is a source of clutter for virtually every type of radar (Miller et al. 1997; Cho 2017). When another transmitter operates at sufficient power to be received by a weather radar, numerous types of RFI can result. The most common type of RFI appears along a subset of radials and is due to a mismatched pulse-repetition frequency (PRF) between the weather radar and the other transmission source. At times, RFI can affect large portions of a weather radar scanning volume, causing significant contamination issues.

Each of these phenomena is characterized by similar appearances in radar variable estimates. While reflectivity factor (Z) and radial velocity (v_r) can vary widely between these four, spectrum width (W) and the polarimetric variables (Z_{DR}, ρ_{HV}, and Φ_{DP}) have considerable similarities. In general, spectrum width (a rough measure of turbulence based on the distribution of radial velocities) is low in these targets (below 3 m s^{-1}). Z_{DR} can span the entire range of potential values (-7.9 to +7.9 dB), a characteristic that does not match most targets.

As would be expected for non-hydrometeor targets, ρ_{HV} is generally low (between 0.2 and 0.8), but can still approach 1.0 at times. Finally, Φ_{DP} serves as potentially the most defining characteristic of these four phenomena, consisting of very high values (between 80-360 degrees) and a relatively high standard deviation (i.e., a "noisy" estimate field). The current HCA tends to label the targets of interest below the melting layer as biologicals, big drops, and unknown categories, and dry snow, ice crystals, and unknown within and above the melting layer (see Fig. 2 for an example in chaff). The proposed "inanimate" class would rectify much of those false alarm misclassifications.

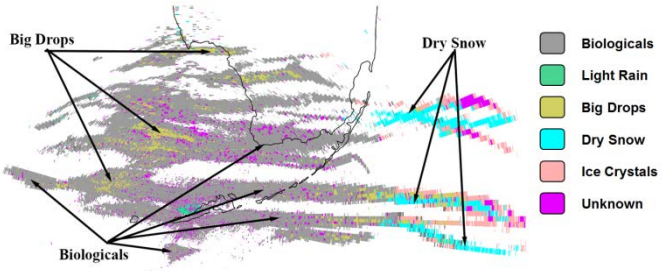

FIG 2: Current HCA output during a chaff release on 12 February 2016 at the KBYX WSR-88D.

3. The Hydrometeor Classification Algorithm

The HCA utilizes the concept of fuzzy logic to determine the most likely target type based on a series of approximate distributions and weights of different variables collected from radar estimates. A quality vector is also applied to determine the reliability of each estimate ingested into the algorithm. In the

WSR-88D implementation, Park et al. (2009) describe the distributions and weights for the six variables that are either directly estimated variables or derived parameters:

- Reflectivity Factor
- Differential Reflectivity
- Cross-Correlation Coefficient
- A Linearized Version of Specific Differential Phase
- Standard Deviation of Reflectivity Factor
- Standard Deviation of Differential Phase

Distributions of the six variables were determined for 10 different target types:

- Ground Clutter/Anomalous Propagation (GC/AP)
- Biological Scatterers (BI)
- Dry Snow (DS)
- Wet Snow (WS)
- Ice Crystals (IC)
- Graupel (GR)
- Big Drops (BD)
- Rain (RA)
- Heavy Rain (HR)
- Rain/Hail Mixture (HA)

These distributions were simplified as non-symmetric trapezoidal functions in either one or two dimensions, convolved with appropriate data quality vectors, related to the altitude of the melting layer, and appropriately weighted to determine the most likely target type for a radar pulse resolution volume.

The HCA method provides a statistical analysis tool to radar users that allows for rapid interpretation of the most likely target by combining much of the available information into a single product. This is especially useful for users who are not as familiar with the intricacies of the dual-polarimetric estimates and desire an easy-to-understand product. The method also provides opportunity for growth into additional target types that have distributions that differentiate them from the existing categories.

The flow of the HCA algorithm is shown in Fig. 3 below. Each of the six variables (shown in blue) has a membership function for each of the 10 target types. Each of these membership functions, ranging from 0 to 1, is multiplied by a corresponding weight (in green) for the variable and target type, as well as a quality vector (in red) for each variable. These values are divided by a summation of the weight and quality vector for normalization according to:

$$A_i = \frac{\sum_{j=1}^{6} W_{ij} Q_j P^i(V_j)}{\sum_{j=1}^{6} W_{ij} Q_j}$$

where A is the aggregate score, W is the weight, Q is the quality vector, and P is the membership function of the variable V. The index j loops across the six variables, while the index i loops across the 10 target types. In order to design a new class, the membership functions and weights must be determined for the six variables such that the new class is reported properly and the existing classes are not improperly changed.

4. Methodology

Of key importance to this study is the collection of large datasets in order to provide enough variety to accurately determine the distributions of radar variables in the inanimate targets. Over the course of 15 months, WSR-88D data from nearly 500

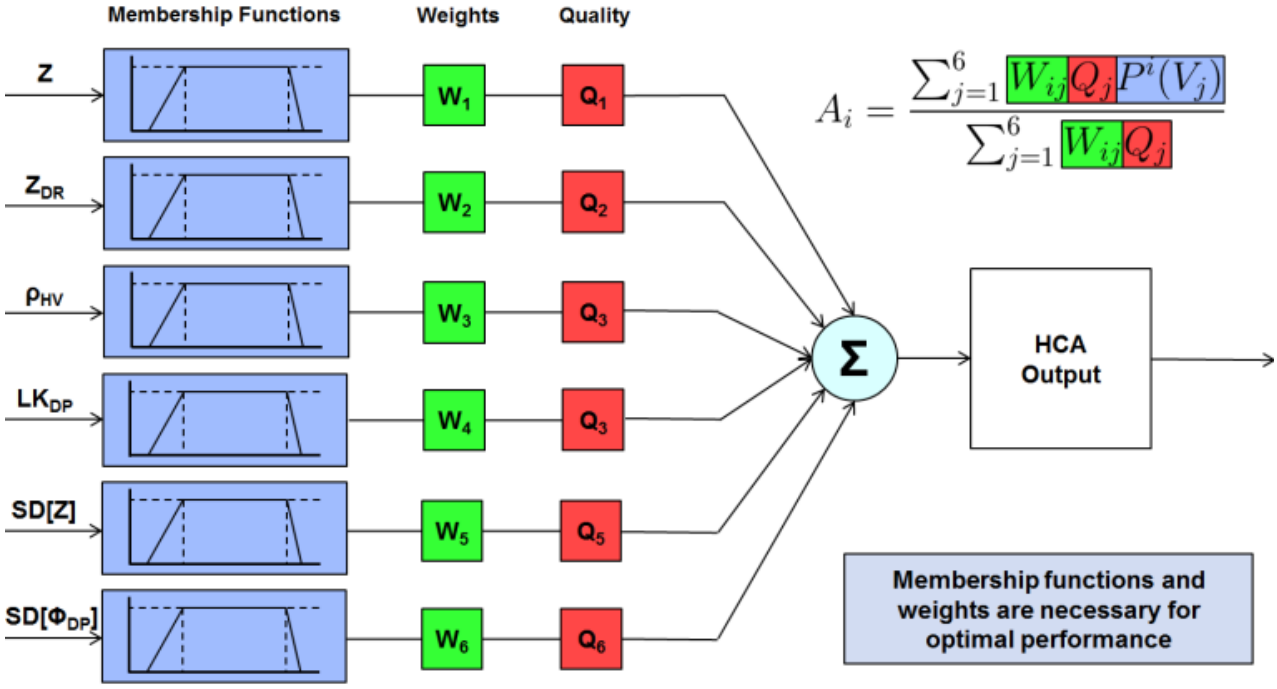

FIG 3: HCA fuzzy logic flow diagram. Membership functions are weighted and convolved with quality vectors before being aggregated to determine the most likely classification.

inanimate cases across the United States were collected. This dataset includes over 2,000 different cells of inanimate targets.

Despite the existence of inanimate scatterers in a radar volume, there are often additional targets such as weather, biological scatterers, and/or clutter. Therefore, the inanimate returns must be manually separated from the non-chaff returns through the use of human truthing. A human-truthing tool originally developed for chaff (Kurdzo et al. 2017) was used to identify cells of inanimate and non-inanimate targets. The tool consists of a simple click-based interface for the user to mark whether a cell or cluster is inanimate or non-inanimate. An example of a chaff case is shown in Fig. 4. A subject matter expert uses all of the available information (i.e., radar variables) to make a decision as to the type of target being observed. After a volume analysis is completed, all of the data associated with inanimates and non-inanimates are stored in a database for future processing.

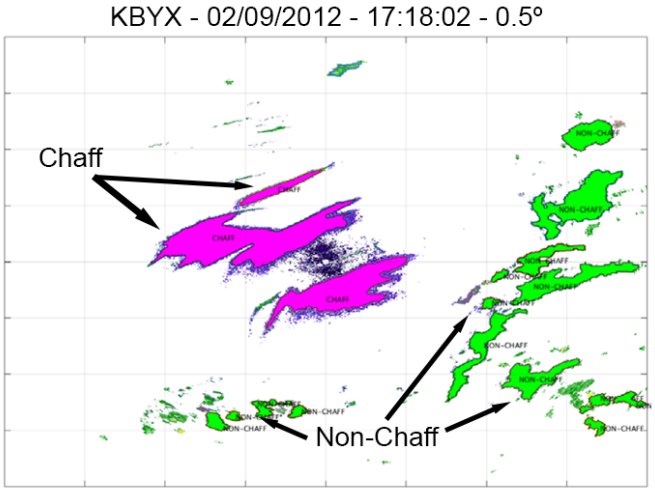

FIG 4: A human-truthing tool for marking chaff and non-chaff was adapted for inanimate cells for this study.

The collection of inanimate cases allows for generation of histogram distributions of the new inanimate class, displaying the typical range of values of the relevant variables (shown in Fig. 5). Note that specific differential phase (K_{DP}) is not shown in Fig. 5 since K_{DP} is not calculated when ρ_{HV} is low, making it irrelevant for this class. In general, Z and Z_{DR} span wide ranges, while ρ_{HV} is exceptionally low, the texture field of Φ_{DP} is exceptionally high, and the texture field of Z is in line with most other targets.

Although these distributions are an accurate portrayal of the variables in inanimate targets, the membership functions in the HCA take the form of simple, non-symmetric trapezoidal functions. Therefore, these functions serve as a starting point for approximate trapezoidal functions that can be input into an optimization algorithm for tuning (Fig. 6). Additionally, no weights have been developed for this new class, so values between 0 and 1 at a resolution of 0.1 are added to the optimization framework.

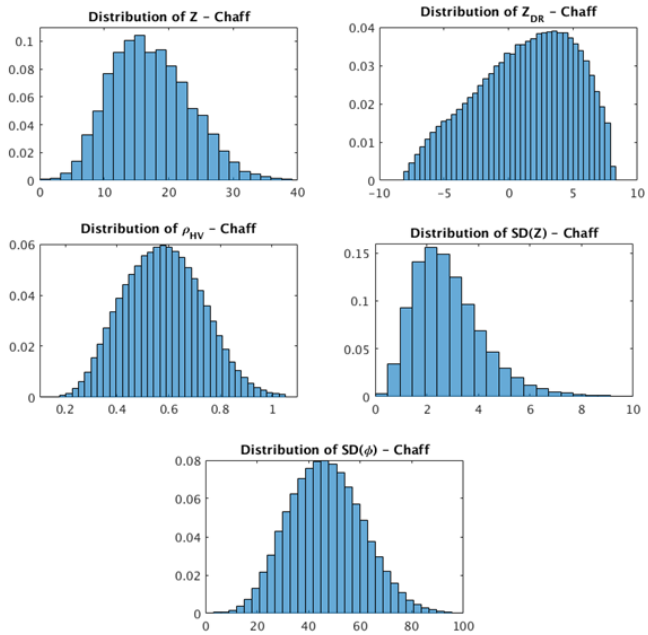

FIG 5: Example distributions of Z, Z_{DR}, ρ_{HV}, and standard deviation of Z and ϕ_{DP} in inanimate cases across the United States.

The optimization scheme chosen is a genetic algorithm, which operates on the theory of evolution. An initial population consisting of at least 30 degrees of freedom (30 variables, including 4 for each of the 6 membership functions and 6 weight values, plus any additional restrictions) is fed to the algorithm and a fitness function is calculated using a standard critical success index. The number of fitness function solutions is based on the population size, resulting in a series of scores. The best

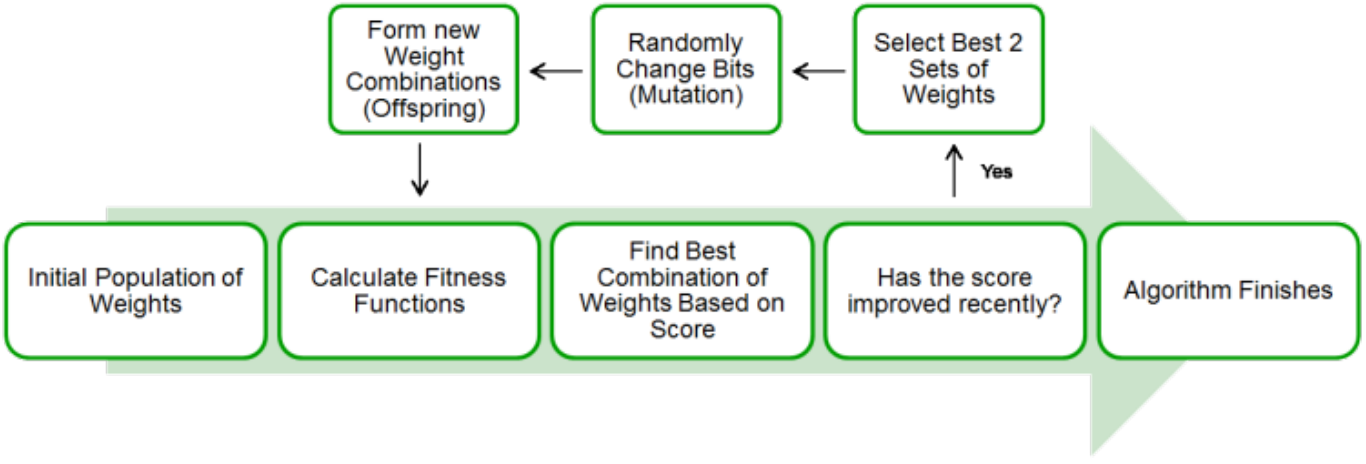

FIG 6: Genetic algorithm flow diagram. The initial population is used to calculate a fitness function value, which is compared with other members of the population. If recent improvement is evident, the population is mutated and the process repeats. A lack of recent change signals completion.

combination is taken, and the score is compared to the previous generation. If the score has improved, the two best populations are selected. Their bits are randomly changed (mimicking mutation in the evolutionary process), and new combinations are made (offspring) in order to define a new population for the succeeding generation. This process continues until the fitness score has "stalled" for a set number of generations, indicating the end of the optimization process.

The goal of the optimization is to maximize the probability of detection for inanimate targets and minimize the false alarm and missed detection rates (i.e., the total number of misclassifications). This is particularly important in the desire to preserve existing classifications that are not inanimate targets. The resulting 24 variables that define the membership trapezoids and 6 variables that define the weights are then used as the basis for a new class in the HCA (along with any additional parameters), which can be tested relative to previous results.

In addition to the 30 "required" variables, a series of additional parameters are included in the optimization. As described in Park et al. (2009), each class has a set of restrictions that disallow their selection under certain circumstances. For example, the ground clutter class is not allowed when the absolute value of radial velocity is greater than 1 m s^{-1}, and the ice crystal class is not allowed when the reflectivity factor is greater than 40 dBZ. A number of possible restrictions were explored for the inanimate class; the chosen fields for restrictions were radial velocity, spectrum width, and the standard deviation (texture field) of Φ_{DP}. In general, if the radial velocity was too low, ground clutter would sometimes be classified as inanimate. If spectrum width was too high, biologicals were often classified as inanimate. Finally, if the standard deviation of Φ_{DP} was too low, general misclassifications took place. Therefore, these three parameters were included in the optimization scheme, resulting in a total of 33 degrees of freedom.

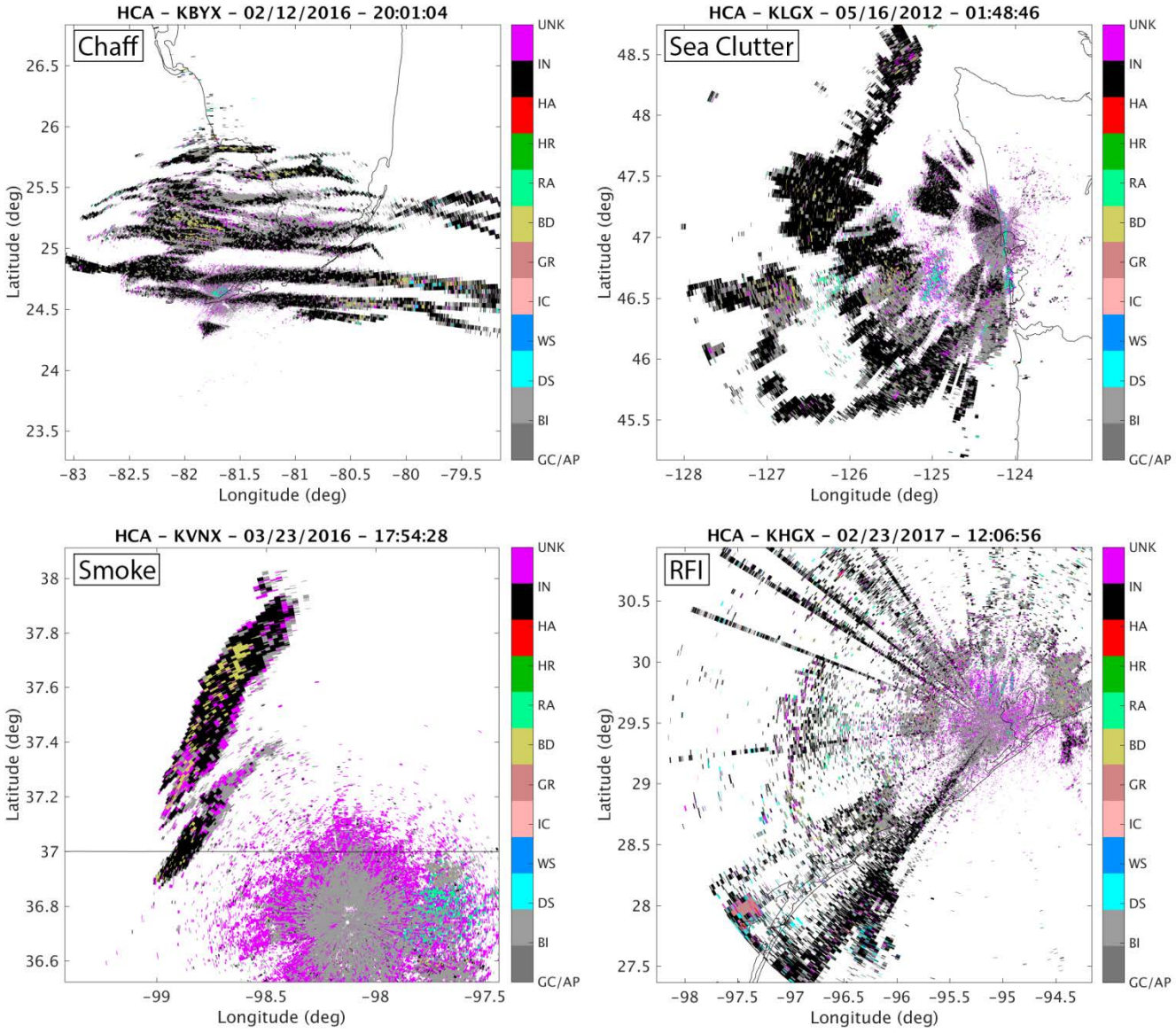

FIG 7: Four case example outputs from the altered HCA with the inanimate classification included. From the top left, clockwise: Chaff at KBYX on 12 February 2016; Sea clutter at KLGX on 16 May 2012; RFI at KHGX on 23 February 2017; and smoke at KVNX on 23 March 2016.

5. Results

The new inanimate classification has been integrated into the existing HCA using an Open Radar Product Generator (ORPG) simulator (Kurdzo et al. 2017). With this tool, any existing Level-II WSR-88D data in the dual-polarimetric era can be ingested and processed with existing and/or modified versions of the current ORPG algorithms. Hundreds of cases have been tested across multiple atmospheric conditions, target types, and locations. One example for each target type in the inanimate class (chaff, sea clutter, smoke, and RFI) is presented in Fig. 7.

The chaff case features multiple horizontally oriented linear segments that originally appeared as mostly biologicals and big drops in the current HCA. Although a non-trivial number of big drop classifications remain, a significant portion of the chaff clouds is labeled as inanimate in the modified HCA. Above the melting layer, some areas of dry snow also remain. Some unknown classifications exist in areas of low signal-to-noise ratio (SNR), especially along the edges of the chaff. The clutter near the radar is not detected as inanimate. Some swaths of biological detections also remain.

The sea clutter case is from the Langley Hill, WA (KLGX) WSR-88D, where the 0.2º elevation angle makes sea clutter a common occurrence. In many of these cases, sea clutter can completely contaminate the western half of the volume at low elevations. In this particular example, much of the sea clutter has been classified as inanimate, but some areas remain classified as biologicals due to anomalously high spectrum widths (>5 m s^{-1}). This is sometimes an issue due to the optimized spectrum width restriction of 2.9 m s^{-1}, but this threshold is necessary for preventiong false alarms in ground clutter.

The example of combustion debris is from a series of large grass fires in northern Oklahoma and southern Kansas. The two discernible smoke plumes were classified as mostly big drops and unknown classes prior to the inanimate addition, primarily due to the size of ash particles. Large areas have been filled in with the inanimate designation. Most of the ground clutter and biological bloom areas are left untouched.

Finally, the RFI case includes multiple radials of interference that feature high and noisy Φ_{DP} estimates. These areas are clearly marked as inanimate classifications, although the mixture of RFI and ducting causes some areas of the clutter bloom to be classified as inanimate. It is important to note that not all types of RFI display the characteristics defined in the inanimate class, so not all RFI cases will be properly detected. This is, in part, due to the fact that some RFI situations look similar to rainfall (due to low values of Φ_{DP}), and attempting to include these cases would likely lead to higher false alarm rates for the inanimate class.

6. Conclusions and Upcoming Work

Multiple non-hydrometeor target types that routinely contaminate the WSR-88D returns are misclassified in the current implementation of the HCA because no suitable class is available for them. For this reason, an inanimate class has been developed for the operational WSR-88D HCA. This class incorporates chaff, sea clutter, combustion debris, and some forms of RFI. Preliminary results show promise for the inanimate class' performance, although statistical measures of probability of detection, probability of false alarm, and missed detection rates will be critical tools in quantifying overall performance.

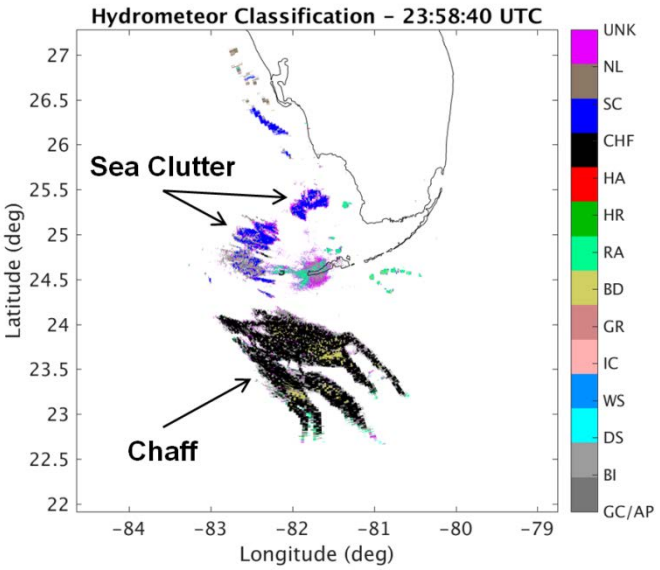

FIG 8: Sample classification between chaff and sea clutter.

Additionally, the National Weather Service and the Federal Aviation Administration have expressed interest the ability to further delineate between the inanimate target types in the form of subclasses. For example, the ability to differentiate between sea clutter and chaff would potentially be useful for both agencies, and such an algorithm could be implemented in various ways. A preliminary look at ongoing work in this area at MIT Lincoln Laboratory is presented in Fig. 8. A support vector machine technique is used as a classifier between chaff and sea clutter. A series of 125 features is used to determine the classification, with features ranging from median, mean, and percentile values of different variables to shapes and edge detection algorithms for clusters of cells. These results are promising for the future and will continue to be explored.

Acknowledgements. Discussions with John Cho, Gabriel Elkin, David Patterson, Brian Klein, Mike Istok, Alexander Ryzhkov, Marilyn Wolfson, and Dusan Zrnić contributed to this work.

REFERENCES

Arnott, W. P. et al., 2004: Determination of Radar Chaff Diameter Distribution, Fall Speed, and Concentration in the Atmosphere by use of the NEXRAD Radar. Desert Research Institute.

Bishop, C., 2007: *Pattern Recognition and Machine Learning*. Springer.

Bringi, V. N. & V. Chandrasekar, 2005: *Polarimetric Doppler Weather Radar: Principles and Applications*. Cambridge University Press.

Chan, H. C., 1990: Radar sea-clutter at low gracing angles. *IEE Proceedings F (Radar and Signal Processing)*, **137**, 102-112.

Cho, J. Y. N., 2017: A new radio frequency interference filter for weather radars. *J. Atmos. Oceanic Technol.*, **34**, 1393-1406.

Crum, T. and R. L. Alberty, 1993: The WSR-88D and the WSR-88D Operational Support Facility. *Bull. of the Amer. Meteor. Soc*., **74**, 1669-1687.

De Martino, A., 2012: *Introduction to Modern EW Systems.* Artech House.

Doviak, R. J. et al., 2000: Considerations for polarimetric upgrades to operational WSR-88D Radars. *J. Atmos. Oceanic Technol.*, **17**, 257-278.

Doviak, R. J. and D. S. Zrnić, 2006: Doppler Radar and Weather Observations. 2nd ed., Dover.

Eiben, A. and J. Smith, 2003: *Introduction to Evolutionary Computing*. Springer.

Hall, P. M., J. W. F. Goddard, and S. M. Cherry, 1984: Identification of hydrometeors and other targets by dual-polarization radar. *Radio Science*, **19**, 132-140.

Harrison, C. and R. Heinz, 1963: On the radar cross section of rods, tubes, and strips of finite conductivity. *IEEE Trans. on Antennas and Propagation*, **11**, 459-468.

Hessemer, R., 1961: Scatter communications with radar chaff. *IEEE Trans. on Antennas and Propagation*, **9**, 211-217.

Holland, J., 1992: *Adaptation in Natural and Artificial Systems*. Cambridge, MIT Press.

Jiusto, J. E. and W. J. Eadie, 1963: Terminal fall velocity of chaff. *J. Geophys. Res.*, **68**, 2858-2861.

Jones, T. A. and S. A. Christopher, 2010: Satellite and radar remote sensing of Southern Plains grass fires: A case study. *J. Appl. Meteor. Climatol.*, **49**, 2133-2146.

Jung, E. and B. Albrecht, 2014: Use of radar chaff for studying circulations in and around shallow cumulus clouds. *J. Appl. Meteor. Climatol.*, **53**, 2058-2071.

Kim, Y. et al., 2013: Real-time detection and filtering of chaff clutter from single-polarization Doppler radar data. *J. Atmos. Oceanic Technol.*, **30**, 873-895.

Krause, J. M., 2016: A simple algorithm to discriminate between meteorological and nonmeteorological radar echoes. *J. Atmos. and Oceanic Technol.*, **33**, 1875-1885.

Kurdzo, J. M. et al., 2017: Polarimetric observations of chaff using the WSR-88D network. *J. Appl. Meteor. and Climatol.*, submitted.

Melnikov, V. M., D. S. Zrnić, R. M. Rabin, and P. Zhang, 2008: Radar polarimetric signatures of fire plumes in Oklahoma. *Geophys. Res. Letters*, **35**, L14815.

Miller, T., L. Potter, and J. McCorkle, 1997: RFI suppression for ultra wideband radar. *IEEE Trans. on Aerospace and Electronic Systems*, **33**, 1142-1156.

Moninger, W. R. and R. A. Kropfli, 1987: A technique to measure entrainment in cloud by dual-polarization radar and chaff. *J. Atmos. Oceanic Technol.*, **4**, 75-83.

Murphy, T. A., R. A. Wade, and B. C. Carcione, 2016: Observations and operational considerations of the 4 June 2013 chaff event in Northern Alabama. *J. Operational Meteor.*, **4**.

Palermo, C. J. and L. H. Bauer, 1965: Bistatic scattering cross section of chaff dipoles with application to communications. *Proc. of the IEEE*, **53**, 1119-1121.

Park, H. A., A. Ryzhkov, D. Zrnić, and K. Kim, 2009: The hydrometeor classification algorithm for the polarimetric WSR-88D: Description and application to an MCS. *Wea. Forecasting*, **24**, 730-748.

Pinson, C. C., 1975: Chaff cloud signature. *IEEE International Symposium on Electromagnetic Compatibility*.

Pode, L., 1960: An approach to the study of automatic target tracking. *Trans. of the AIEE, Part I: Communication and Electronics*, **78**, 806-811.

Ryzhkov, A. V. et al., 2005: The Joint Polarization Experiment: Polarimetric rainfall measurements and hydrometeor classification. *Bull. Amer. Meteor. Soc.*, **86**, 809-824.

Snyder, J. C. and A. V. Ryzhkov, 2015: Automated detection of polarimetric tornadic debris signatures using a hydrometeor classification algorithm. *J. Appl. Meteor. Climatol.*, **54**, 1861-1870.

Torres, S. M. and D. A. Warde, 2014: Ground clutter mitigation for weather radars using the autocorrelation spectral density. *J. Atmos. Oceanic Technol.*, **31**, 2049-2066.

Torres, S. M. and D. S. Zrnić, 1999: Ground clutter canceling with a regression filter. *J. Atmos. Oceanic Technol.*, **16**, 1364-1372.

Weinheimer, A. J. and A. A. Few, 1987: The electric field alignment of ice particles in thunderstorms. *J. Geophys. Res.*, **92**, 14,833-14,844.

Yu, J., H. Lee, Y. Jeong, and S. Kim, 2016: Identifying chaff echoes in weather radar data using tree-initialized fuzzy rule-based classifier. *IEEE International Conference on Fuzzy Systems*.

Zrnić, D. and A. Ryzhkov, 2004: Polarimetric properties of chaff. *J. Atmos. Oceanic. Technol.*, **21**, 1017-1024.

Zrnić, D. S. and A. V. Ryzhkov, 1999: Polarimetry for weather surveillance radars. *Bull. of the Amer. Meteor. Soc.*, **80**, 389-406.